Hands-on Session: Disk Modelling

Virginie Faramaz (JPL, Caltech/IPAC-NExScI)

Elise Furlan (Caltech/IPAC-NExScI), Karl Stapelfeldt (JPL),
Chas Beichman (Caltech/IPAC-NExScI), Christine Chen (STScI)

1 INTRODUCTION

This hands-on session will introduce you to circumstellar disks, how they are studied, how they appear at different stages of their evolution, and the different features they can exhibit.

SPECTRAL ENERGY DISTRIBUTION (SED) AND IMAGES   You will first get acquainted with the concept of the SED (Figure 1), which represents how bright a source is as a function of wavelength. Historically, and before any detailed images of disks were obtained, circumstellar disks were identified around a wide variety of stellar types because the surrounding dust absorbs starlight and re-radiates that energy in the infrared, resulting in excess infrared (IR) emission above the stellar photospheric emission (see Figure 2).
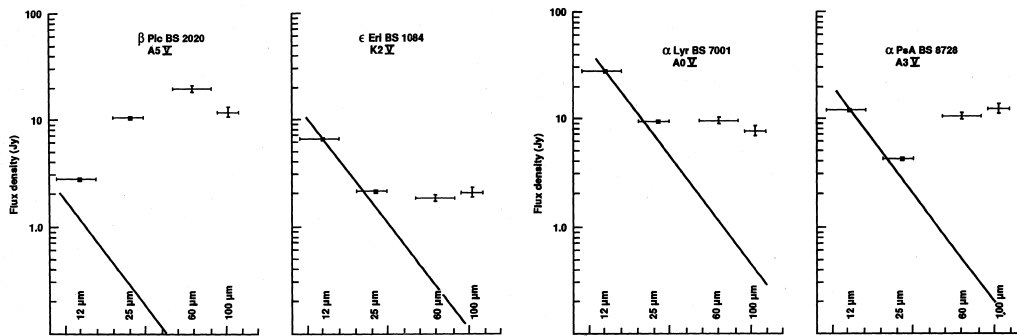

Figure 1: An SED model of a star surrounded by a circumstellar disk
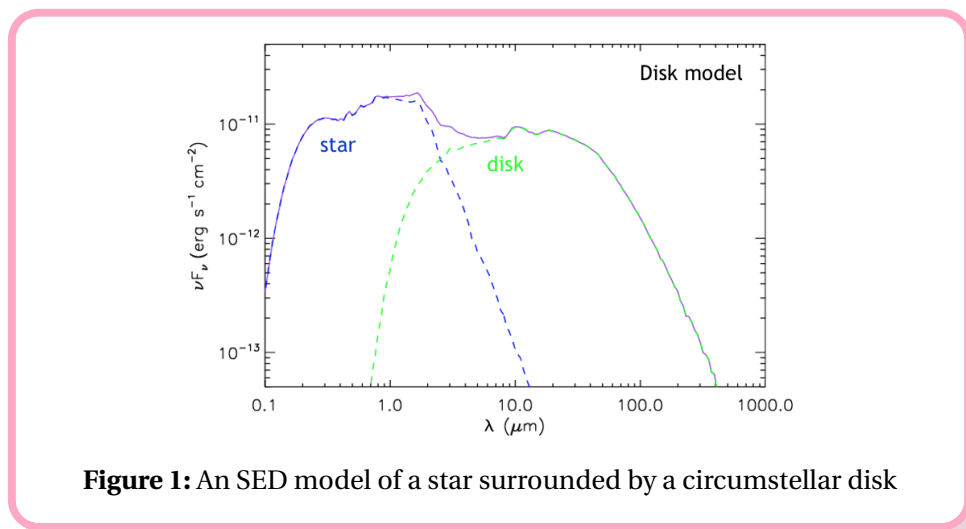
Figure 2: SEDs of the "Fabulous Four", the debris disks of Beta Pictoris, Epsilon Eridani, Vega (α Lyrae), and Fomalhaut (α Piscis Austrini) (from left to right, respectively; from Backman & Paresce, 1993). These show photometric measurements taken with the Infrared Astronomical Satellite (IRAS) at infrared wavelengths. The solid line is the tail of the star's blackbody emission. One can clearly see that the IR emission exceeds that expected from the star; this is a sign that the star harbours circumstellar dust. These were the first four debris disks discovered.

The IRAS satellite, launched in 1983, discovered excess IR emission from a number of main-sequence stars, including the prototypical A star, α Lyrae (Vega), leading to this class of circumstellar or debris disks being called the Vega Phenomenon (Aumann et al., 1984; Backman & Paresce, 1993). After the initial IRAS discovery, Smith & Terrile (1984) made a coronagraphic image of Beta Pictoris which revealed the presence of an edge-on disk (see Figure 3).
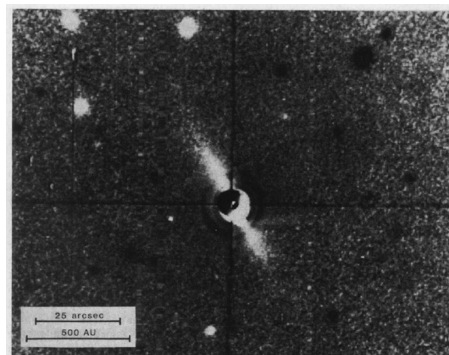

Figure 3: Coronagraphic image of Beta Pictoris (Smith & Terrile, 1984). This was the first resolved image of a debris disk.

Subsequent IR facilities (ISO and Spitzer, launched in 1995 and 2003, respectively) greatly expanded the number and provided insight into the nature of known disks through their reradiated emission at IR wavelenghts and their SED.

On the other hand, our knowledge of disks also dramatically improved as new facilities were able to provide images of those disks. In particular, advanced coronagraphic imaging from the Hubble Space Telescope (HST) led to vast improvements in our knowledge of the disks in scattered starlight, that is, at optical and near-infrared wavelengths (see Figure 4). There are also recent ground-based coronagraphic imaging instruments, aided by the use of adaptive optics, that enable us to obtain high-resolution images of debris disks (see Figure 5).
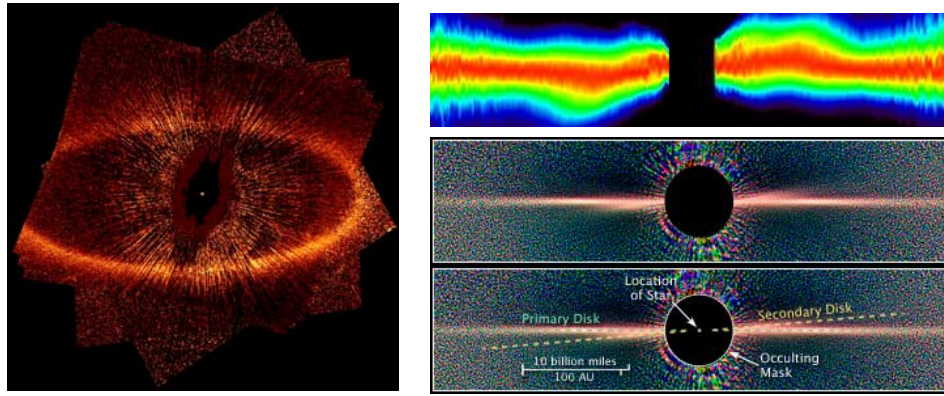
Figure 4: HST/STIS image of the debris disk of Fomalhaut (*left;* Kalas et al., 2005). HST images of the debris disk of Beta Pictoris, with STIS (*top right;* Heap et al., 2000) and ACS (*bottom right* Golimowski et al., 2006). Fomalhaut appears offset from the disk center of geometry, i.e., the disk is intrinsically eccentric. The debris disk of Beta Pictoris exhibits a warp, i.e., a secondary disk mutually inclined with the main one. In both cases, these large scale asymmetries indicate the presence of planet(s) dynamically sculpting those disks.
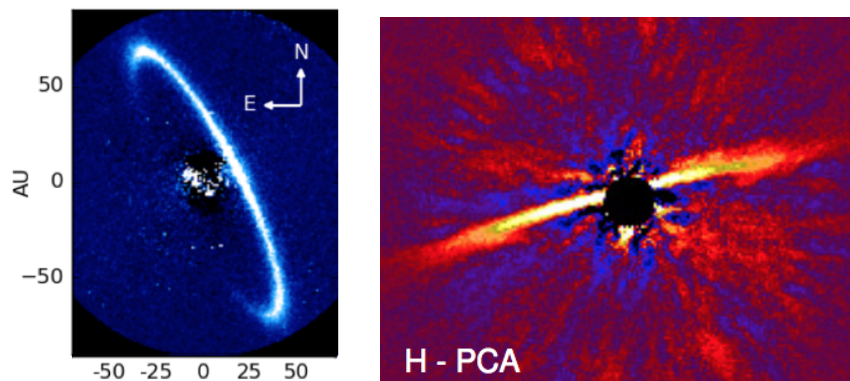

Figure 5: Gemini Planet Imager (GPI) image of the debris disk of HR 4796 in the J-band (1.24 μm) (*left;* Arriaga et al., 2020). VLT/SPHERE image of the debris disks of HD 106906 in the H-band (1.6 μm) (*right;* Lagrange et al., 2016).

Resolved images of many disks' thermal emission at IR and (sub)millimeter wavelengths were provided by facilities such as the Herschel Space Observatory, the James Clerk Maxwell Telescope (JCMT), and the Atacama Large Millimeter Array (ALMA); examples are shown in Figure 6.
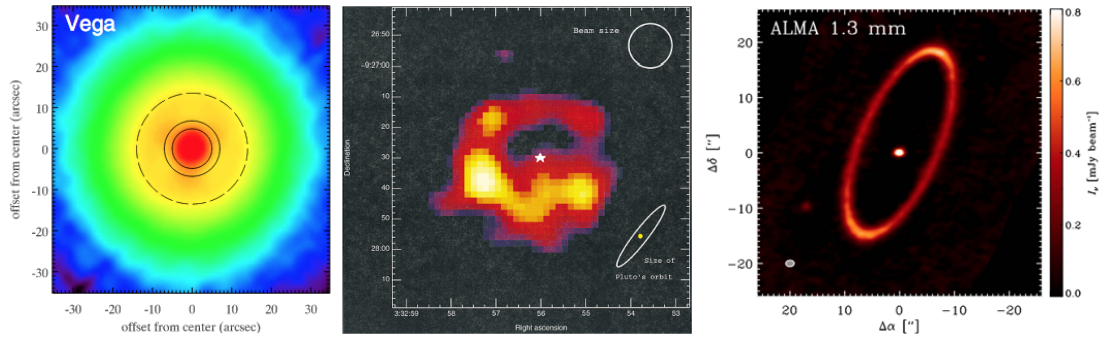
Figure 6: Herschel/PACS 70 μm image of the debris disk of Vega (*left;* Su et al., 2013), JCMT 850 μm image of the debris disk of Epsilon Eridani (*middle;* Greaves et al., 1998), and ALMA 1.3 mm map of the debris disk of Fomalhaut (*right;* MacGregor et al., 2017).

Find these images and many more in the online catalog of spatially resolved circumstellar disks, available at https://circumstellardisks.org.

BIRTH AND EVOLUTION OF DISKS   In addition, stars are known to be born in molecular cloud cores, surrounded by large envelopes of dust and gas. This circumstellar material also causes excess emission at IR and longer wavelengths and often obscures the forming star at optical wavelengths. The material from the envelope surrounding a young protostar falls onto a disk and is accreted from there onto the star. Some of the accreting material is also ejected in outflows aligned with the rotation axis of the star, perpendicular to the disk plane.

Over the course of a few hundred thousand years, the envelope is depleted, and the young star is left with its circumstellar accretion disk (see, e.g., Figure 7). These stars are also known as T Tauri stars, after the prototype star T Tau in the Taurus star-forming region. During this phase, the star continues to accrete material, and both the gas and dust in the disk evolve. In particular, small dust grains grow and settle towards the disk midplane, causing the disk to be less flared (smaller scale height), thus intercepting less starlight and emitting less infrared radiation.
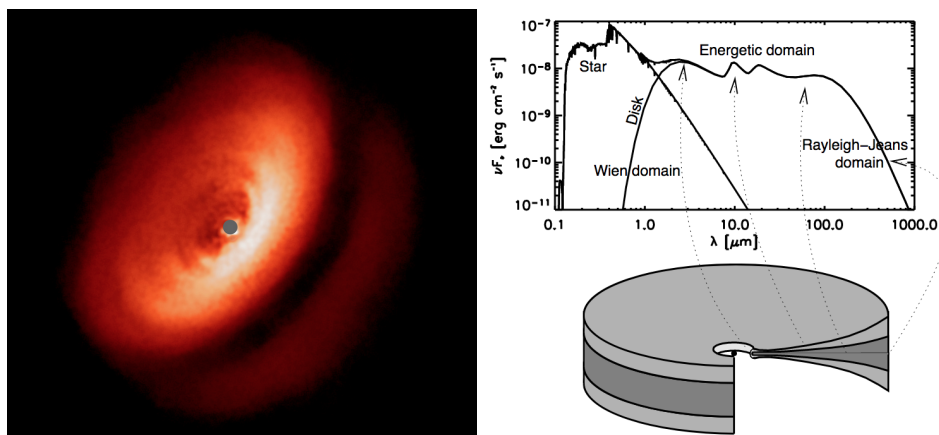

Figure 7: *Left:* H-band image of IM Lup obtained with the VLT; it is a T Tauri star surrounded by a large, flared disk (Avenhaus et al., 2018). *Right:* Schematic of a flared disk and its SED (Dullemond et al., 2007)

4

The primordial or protoplanetary disks around T Tauri stars are also thought to be the birth-places of planets; as planets form and grow, they clear gaps in the disk (see Figure 8). After a few million years, the protoplanetary disk is dispersed due to various processes, and eventually the star becomes a main-sequence star. It is around main-sequence stars that debris disks are formed from collisions of planetesimals left over from the planet formation process.

This entire temporal evolution sequence is outlined in Figure 9, and Figure 10 shows the evolution of a protoplanetary disk, from flared to settled, which includes the growth of larger bodies, and finally disk dispersion.
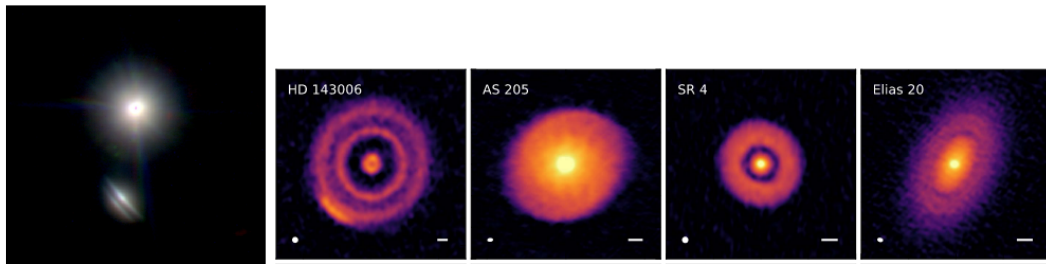

Figure 8: *Left:* VLT J-, H-, and K-band three-color image of the HK Tau binary (McCabe et al., 2011). *Right four images:* Protoplanetary disks observed by ALMA at 1.3 mm (Andrews et al., 2018)
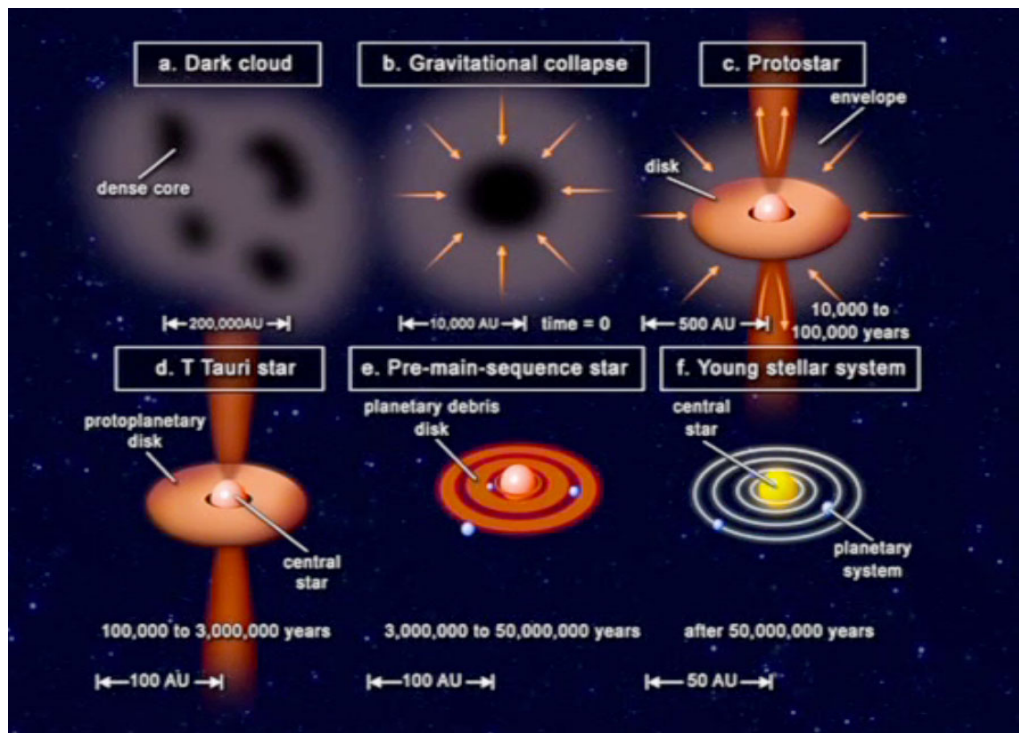

Figure 9: Phases of star and planetary system formation (schematic by Tom Greene, 2001).
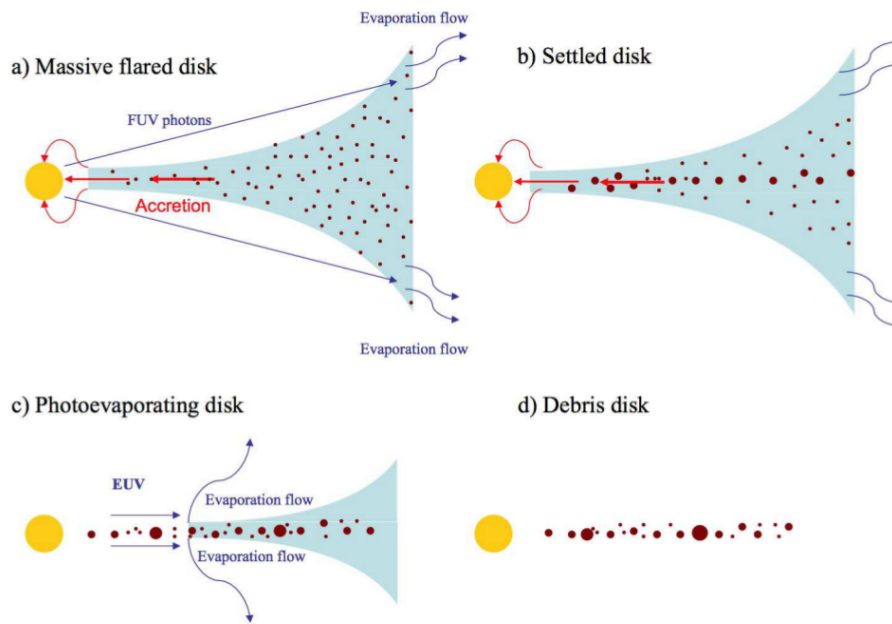
Figure 10: The evolutionary stages of a protoplanetary disk. The typical lifetime of protoplanetary disks is estimated to be less than 10 million years (Myr). The flaring of the disk is due to hydrostatic balance (Williams & Cieza, 2011)

In this hands-on session, you will discover what kind of information astronomers retrieve from SEDs and images and how these two different products complement each other.

THE PROTAGONISTS We have selected four objects that are each representative of different evolutionary stages of star and planetary system formation. Here is a short introduction for each of those to help you choose which ones (or all of them!) you would like to explore:

- **HL Tau:** Not only does HL Tau harbour a protoplanetary disk, but it is also still surrounded by a large envelope of gas and small grains (stage (c) in Fig. 9). It became famous when ALMA pierced through the envelope and revealed that the largest grains in the disk, detected at millimeter wavelengths, harbored a series of gaps.
- **Herbig-Haro 30:** This young stellar object hosts an edge-on protoplanetary disk in which the large dust grains have settled onto the disk midplane into a flat structure, while the smaller grains exhibit a less flattened and more flared distribution. In addition, this system displays a jet (stage (d) in Fig. 9, and stage (b) in Fig. 10).
- **PDS 70:** This star harbours what we call a transition disk, characterized by the presence of a large central cavity carved out by some combination of stellar wind, radiation pressure, grain growth, accretion of primordial material onto the star, or perhaps even forming planets. PDS 70 harbours two giant planets within the cavity. This corresponds roughly to stage (e) in Fig. 9) and stage (c) in Fig. 10.
- **HR 4796:** This is what we call a debris disk, analogous to the objects first discovered by IRAS (and shown in Fig. 2 to 6). It is much less massive than a protoplanetary disk and has little or no gas; it is dominated by a second generation of dust generated by collisions of large remnant bodies (asteroids and comets, like in the Solar System's asteroid and Kuiper Belts). The material in this particular debris disk resides in a narrow ring, perhaps shepherded by the presence of one or more planets, while other debris disks show a much broader distribution. This corresponds to stage (f) in Fig. 9) and stage (d) in Figure 10.

THE SCIENCE QUESTIONS   There is a lot of information on the structure, intrinsic properties, and evolutionary stage of a circumstellar disk that can be retrieved from the examination of an SED and/or an image. We're saying "and/or" because sometimes information can be simply retrieved from the SED, and sometimes images are required to alleviate degeneracies and pinpoint the exact origin of the SED's characteristics.

In other words, you will investigate science questions of the following type:

- **What can an SED tell me about X for this specific system? And what do images tell me about X? (Where X is a certain property)**
- **Do I need an image to complement the SED or is the SED sufficient to retrieve the information I need?**
- **Is there an underlying physical phenomenon at play?**

The X can be the inclination at which the system is seen, the mass of its circumstellar disk, the presence of a planet, the disk structure, etc... In Table 1, we list the parameters and properties explored and which one of the four selected objects will allow you to know more about them.

Property explored	Object			
	HL Tau	**HH 30**	**PDS 70**	**HR 4796**
Envelope Mass				
Presence of Gaps				
Scale Height				
Inclination				
Flaring				
Disk Mass				
Cavity Size				
Cavity Depth				
Presence of a Planet				
Distance of Dust from Star				
Dust Grain Size				

Table 1: Disk/system properties explored in this hands-on session and which one of the four selected objects allows you to explore them.
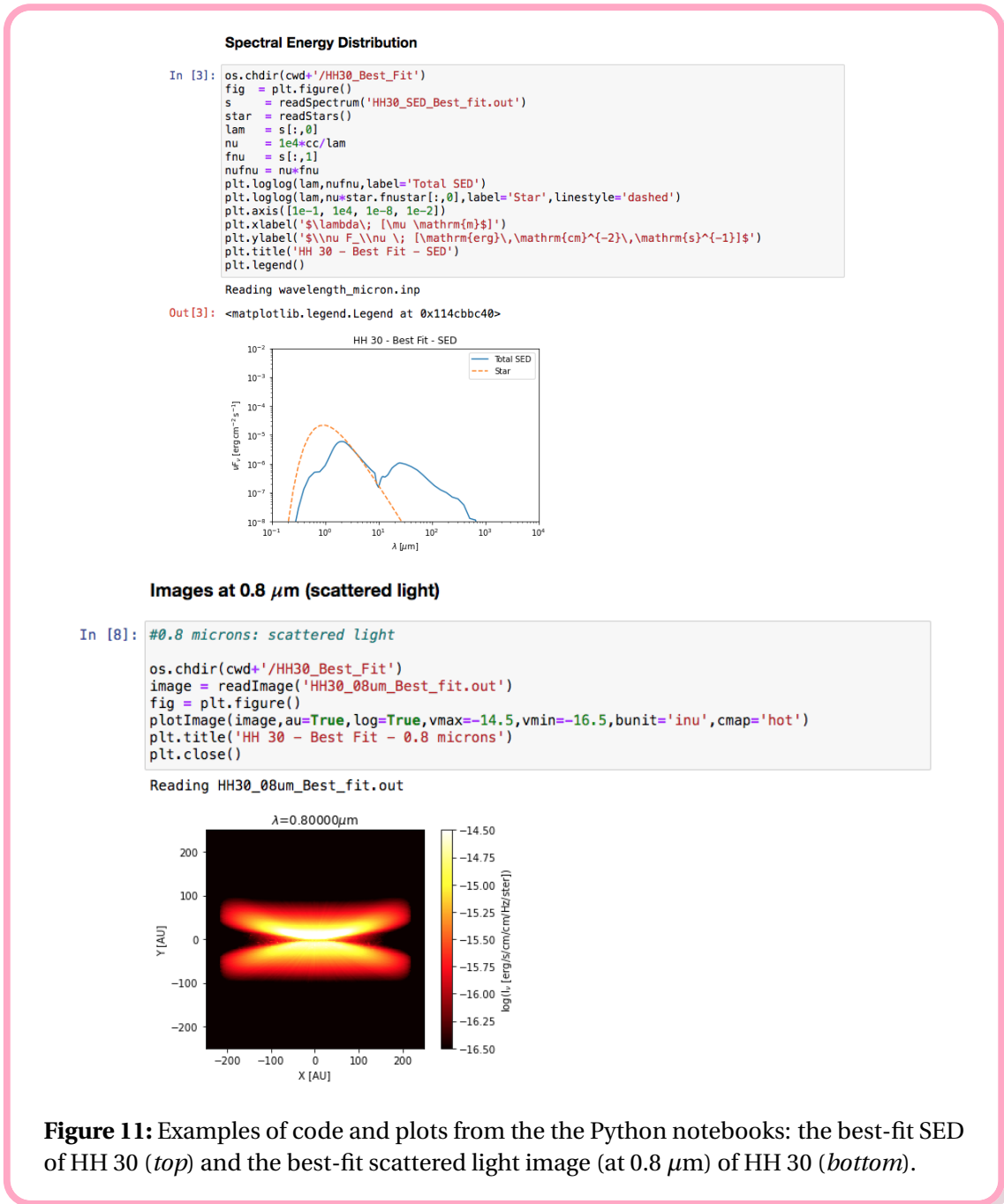
HOW YOU ARE GOING TO STUDY DISK PROPERTIES   During this session, you will be provided with the outputs of a radiative transfer code called RADMC-3D, developed by Cornelis P. Dullemond. This is a code which, given stellar and disk parameters, allows one to compute how the disk dust grains interact with the light from the star, either reflecting it (scattered emission) or absorbing and re-emitting it (thermal emission). The code produces images of the disk at a given wavelength and for a given orientation. The code also produces the SED of the system.

The production of these images and SEDs can require complex installations (depending on your operating system) and, most importantly, can take a significant amount of time to produce a single model. Therefore, because we want you to make the best out of your time in this session, we will not ask you to compute those products yourselves, but rather we will provide the end products for you to analyze. Note that as part of the software installation for this hands-on session, you will install RADMC-3D, but we will only use its Python plotting routines.

The end products of RADMC-3D (images and SEDs) can be plotted using a set of Python tools. If you are not acquainted with Python's ability to produce plots for your publications and reports, this hands-on session will also provide a good introduction to its capabilities. You will

use Jupyter notebooks to read in the model files and plot them (see Figure 11 for an example). For each disk, you will execute the cells in the Jupter notebook to plot the SEDs and images, and, to explore the effect of changing certain parameters, you will copy the lines with the plotting commands into new cells to plot different model files. Alternatively, we make Google Colab notebooks available, which are similar to the Jupyter notebooks, but do not requite a Python installation and instead run in your Google Drive, using a free virtual machine.

Please check the Installation documents to find information to either install Python on your computer or how to use the Google Colab notebooks. These are available here.

Figure 11: Examples of code and plots from the the Python notebooks: the best-fit SED of HH 30 (*top*) and the best-fit scattered light image (at 0.8 μm) of HH 30 (*bottom*).

2 HL Tau

INTRODUCTION   HL Tau is a young stellar object in the Taurus star-forming region, about 140 pc away. At an age of about 1 Myr, it is still surrounded by an infalling envelope, which feeds gas and dust onto a circumstellar accretion disk (Figure 12). In 2015, high-resolution ALMA images of the sub-mm and mm emission revealed that the disk has several gaps (Figure 13); they could be caused by giant planets forming in the disk, a change in dust properties, and gravitational instabilities. Those gaps are present not only in the dust emission, but also in the gas (right panel of Figure 14), which lends more weight to the theory that planets clear these gaps due to tidal interactions with the disk. It also has jets and outflows that lie perpendicular to the disk.
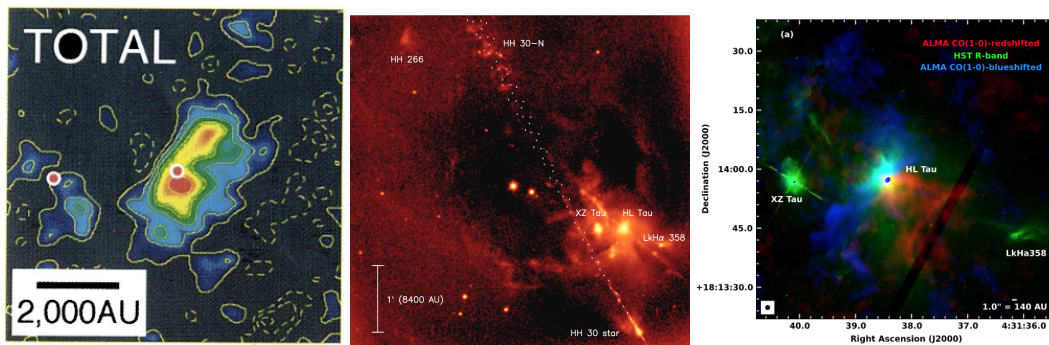

Figure 12: Views of the envelope around HL Tau. **Left:** Envelope around HL Tau imaged in the ^{13}CO emission at 2.7 mm (Hayashi et al., 1993). **Middle:** Nordic Optical Telescope images of the HL Tau region taken in the [SII] filter (672 nm); other young stellar objects, like XZ Tau, HH 30, and LkHa 358 are also included (Anglada et al., 2007). **Right:** ALMA ^{12}CO and HST R-band image of HL Tau (ALMA Partnership et al., 2015).
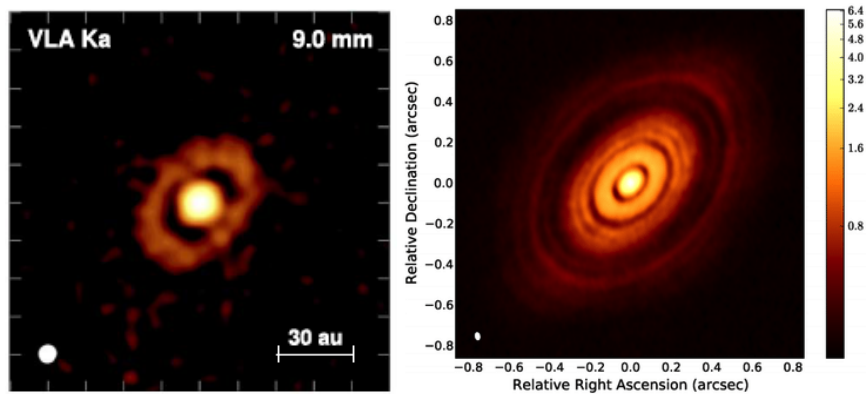

Figure 13: Views of the protoplanetary disk surrounding HL Tau, which is embedded inside the envelope. **Left:** VLA 9 mm low-resolution continuum map of HL Tau (Carrasco-González et al., 2019). **Right:** ALMA 1.3 mm continuum high-resolution map of the disk of HL Tau (ALMA Partnership et al., 2015).
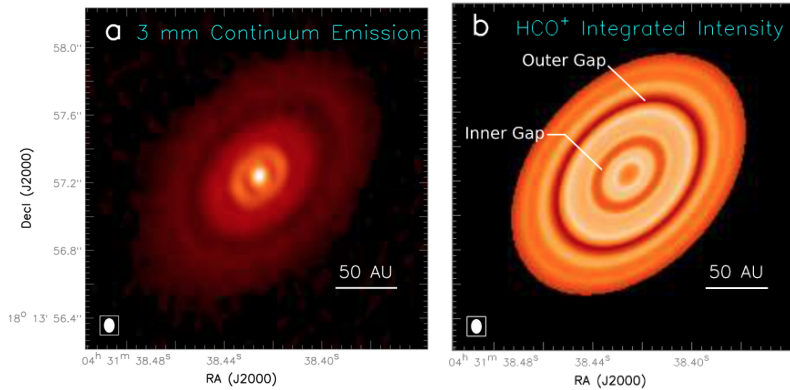
9

Figure 14: The disk gaps of HL Tau: 3 mm continuum image (**left**) and HCO$^+$ image (**right**) (Yen et al., 2016).

RADMC-3D MODEL - IMPORTANT FEATURES: The star is taken as a blackbody of temperature 4,000 K and modeled as a point source. The system is seen 47° from face-on and is made up of three components. First, the envelope: it is approximated as spherical, and so its geometry is parameterized by only its radius; its density is defined by a **central density** ρ_0 and a power law index γ. The code does not allow for a cut-off at a given distance, but even though envelopes typically extend over scales of several 1,000 AU, the outer parts are tenuous and cold, and therefore it is sufficient for the output images here to be limited to 1,000 AU in radius.

Hidden inside the envelope, the protoplanetary disk is made up of two sub-disks, both extending from 0.2 to 120 AU. One disk is made of large, 100 μm grains, which have settled in the mid-plane; therefore, its **scale height** is taken to be 1%, with a reference distance of 100 AU. This means that the disk is taken to be 1 AU thick at 100 AU. This is the disk that exhibits the gaps seen in the famous ALMA image. Another disk component of smaller 0.1 μm grains does not exhibit the gaps and has not settled to the mid-plane: its scale height factor is taken to be 0.15 (or 15%, corresponding to a disk vertical extent of 15 AU at a radius of 100 AU).

PYTHON NOTEBOOKS: To study this object, you will work through a Python notebook (either a Jupyter notebook, if you have installed Python, or a Google Colab notebook) and plot various model SEDs and model images (see Figure 15 for an example).
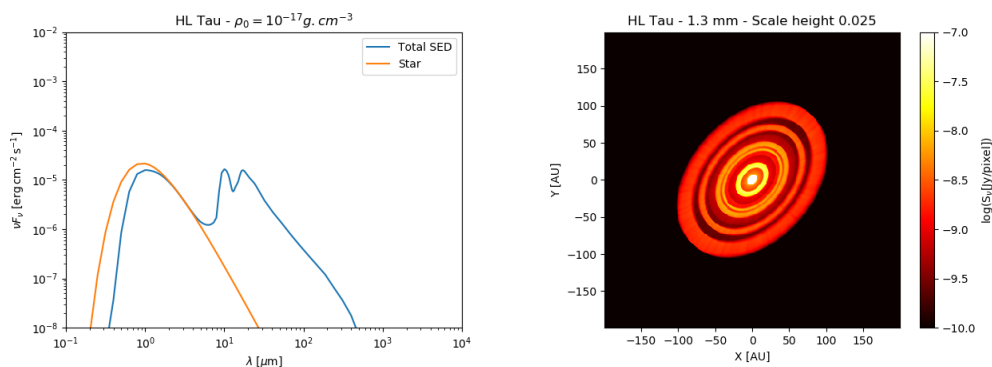

Figure 15: Examples of a model SED plot (**left**) and model image (**right**) for HL Tau. These are the type of plots you will generate in the Python notebook.

As you work through the Python notebook, you will explore the effect of the envelope mass, the presence of gaps, and disk scale height. Please be ready to address the following questions:

QUESTIONS

1. How does the mass of the envelope (set by its initial density) affect the images of the system at visible wavelengths?
2. And how does it affect the SED? **If you have also studied HH 30:** can you derive the presence of an envelope from the SED only or is there another parameter you can think of that can produce the same type of effect on the SED?
3. Can an SED be used to infer the presence of gaps?
4. Can an SED be used to derive the disk scale height?
5. Can the disk scale height be retrieved from images if the disk is seen at certain inclination angles?

3 HH 30

Introduction HH 30 is a young stellar object in the Taurus star-forming region, about 140 pc away. It is about 1 Myr old and surrounded by an accretion disk, which feeds material onto the star. The disk of HH 30 is seen edge-on. HH 30 drives a jet, which is launched perpendicular to the disk (see left panel of Figure 16). Large dust grains have settled into the disk midplane, while smaller grains are found at larger scale heights, delineating a flared disk surface. This flared disk can be seen in reflected light in the near-infrared (see middle panel of Figure 16).
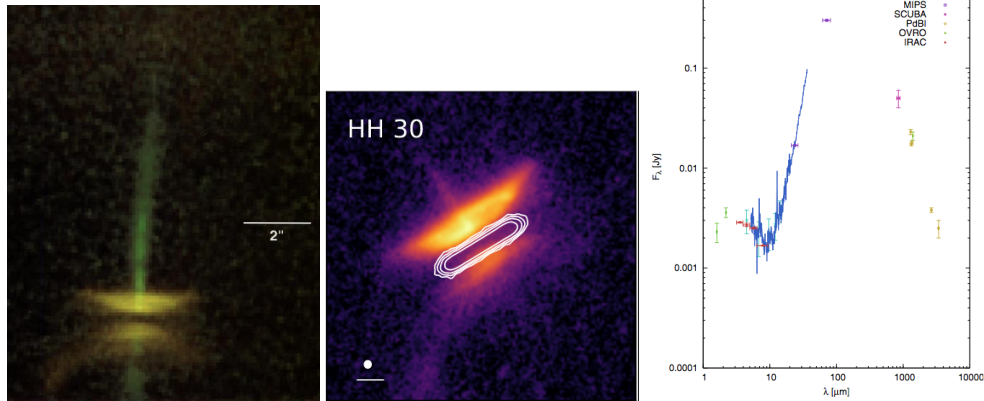

Figure 16: Left: False-color HST/WFPC2 image at optical wavelengths of HH 30 (Burrows et al., 1996). **Middle:** ALMA continuum map at 0.89 mm (contours) superposed on the HST data; the bar in the bottom left corner indicates a scale of 0.5" (Villenave et al., 2020). **Right:** SED of HH 30 (Madlener et al., 2012).

Radmc-3D Model - Important Features: The star is taken as a blackbody of temperature 4,000 K. The disk model consists of two sub-disks, both extending from 0.2 AU to 220 AU, for a **total dust mass** of $6 \times 10^{-3} \, M_\odot$. One disk is made of large (100 μm) grains that have settled in the midplane (scale height factor is 0.01) and which represent 99% of the disk dust mass. The other disk is made of small 0.1 μm grains which have not settled to the midplane (scale height factor of 0.15) and present a flared distribution, with a **flaring index** of 0.4; it contains 1% of the disk's total dust mass. The flaring index ξ is defined such that $\frac{H}{R} \propto R^{1+\xi}$, where H is the height of the disk surface and R is the disk radius. The whole system is seen with an **inclination** angle of 84° from face-on.

Python Notebooks: To study this object, you will work through a Python notebook (either Jupyter notebook, if you have installed Python, or a Google Colab notebook) and plot various model SEDs and model images (see Figure 17 for an example).
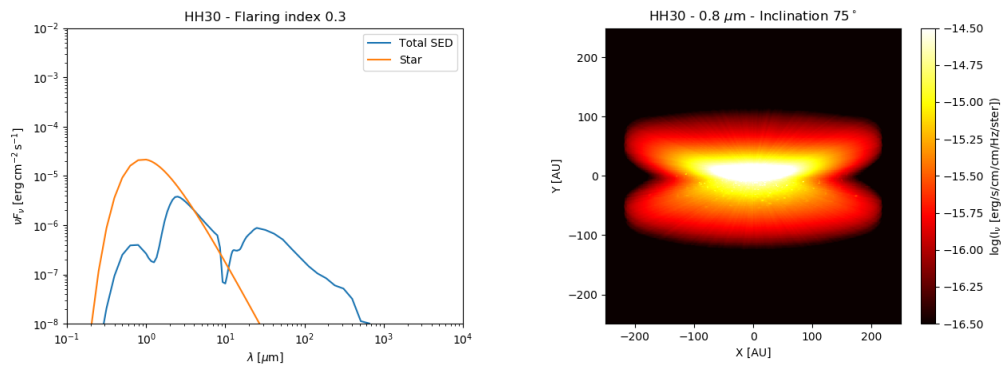
Figure 17: Examples of a model SED plot (**left**) and model image (**right**) for HH 30. These are the type of plots you will generate in the Python notebook.

As you work through the Python notebook, you will explore the effect of the disk mass, inclination angle, and flaring index. Please be ready to address the following questions:

QUESTIONS

1. How does the inclination of the system affect the images of the system at visible wavelengths?
2. And how does it affect the SED? What is the physical phenomenon at play?
3. How does the mass of the disk affect the images of the system at visible and sub-millimeter wavelengths?
4. And how does it affect the SED? What is the physical phenomenon at play?
5. How does the flaring of the disk affect the images of the system at visible wavelengths?
6. And how does it affect the SED? What is the physical phenomenon at play?
7. Can you infer any of these three properties (inclination angle, disk mass, flaring of the disk) from the SED only?

4 PDS 70

INTRODUCTION   PDS 70 is a pre-main-sequence star located in the Upper Centaurus-Lupus group at a distance of about 113 pc and has an age of about 5 Myr. It is surrounded by a pre-transition disk, which is a disk that has a large inner gap that was cleared due to disk evolution (see Figure 18). This gap manifests itself by a reduction in infrared emission in the SED. In most pre-transition and transition disks, the inner cavity is cleared of dust, but there is still remnant gas, which keeps accreting onto the star. Several factors can cause disk clearing, among them photoevaporation by the central star, grain growth, and forming planets. The inner cavity in PDS 70 is quite large, with a radius of about 70 AU; in near-infrared scattered light, the outer disk edge is located at 140 AU (see left panel of Figure 19). Sub-mm images reveal a ring of dust, extending from about 60 to 110 AU from the star (see right panel of Figure 19).
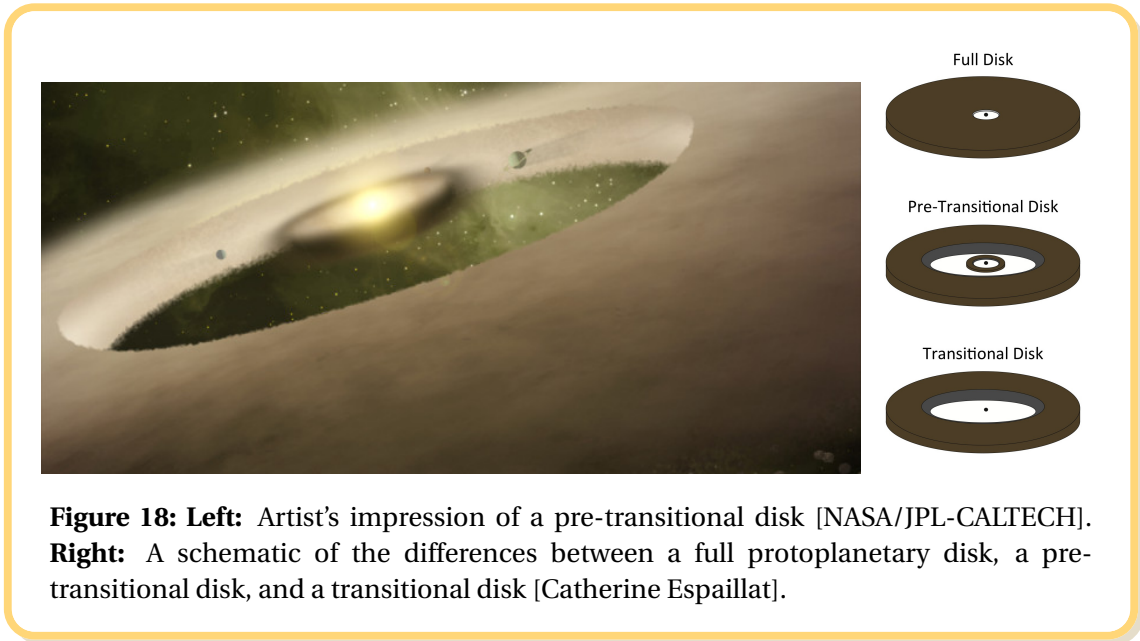

Figure 18: Left: Artist's impression of a pre-transitional disk [NASA/JPL-CALTECH]. **Right:** A schematic of the differences between a full protoplanetary disk, a pre-transitional disk, and a transitional disk [Catherine Espaillat].
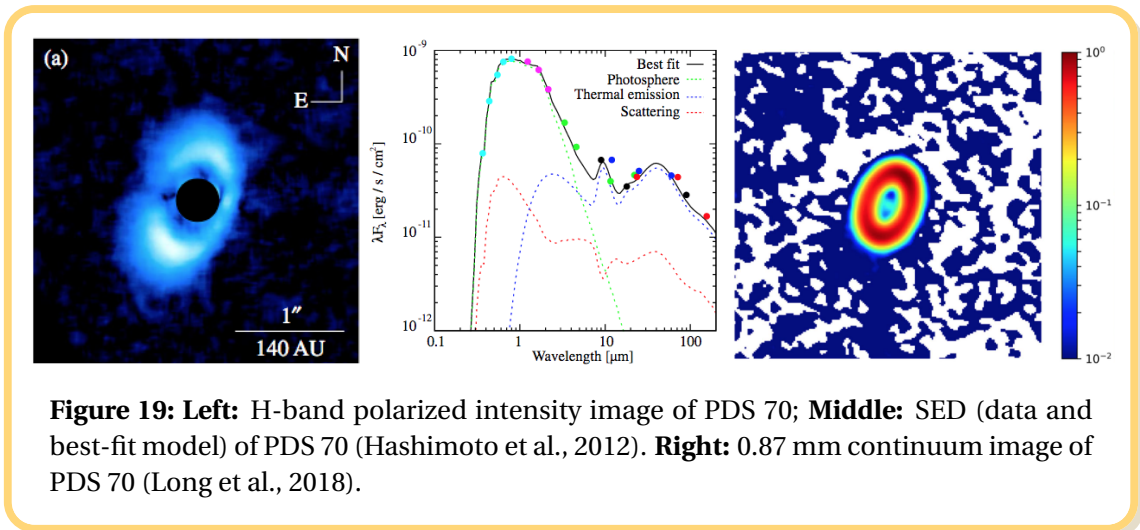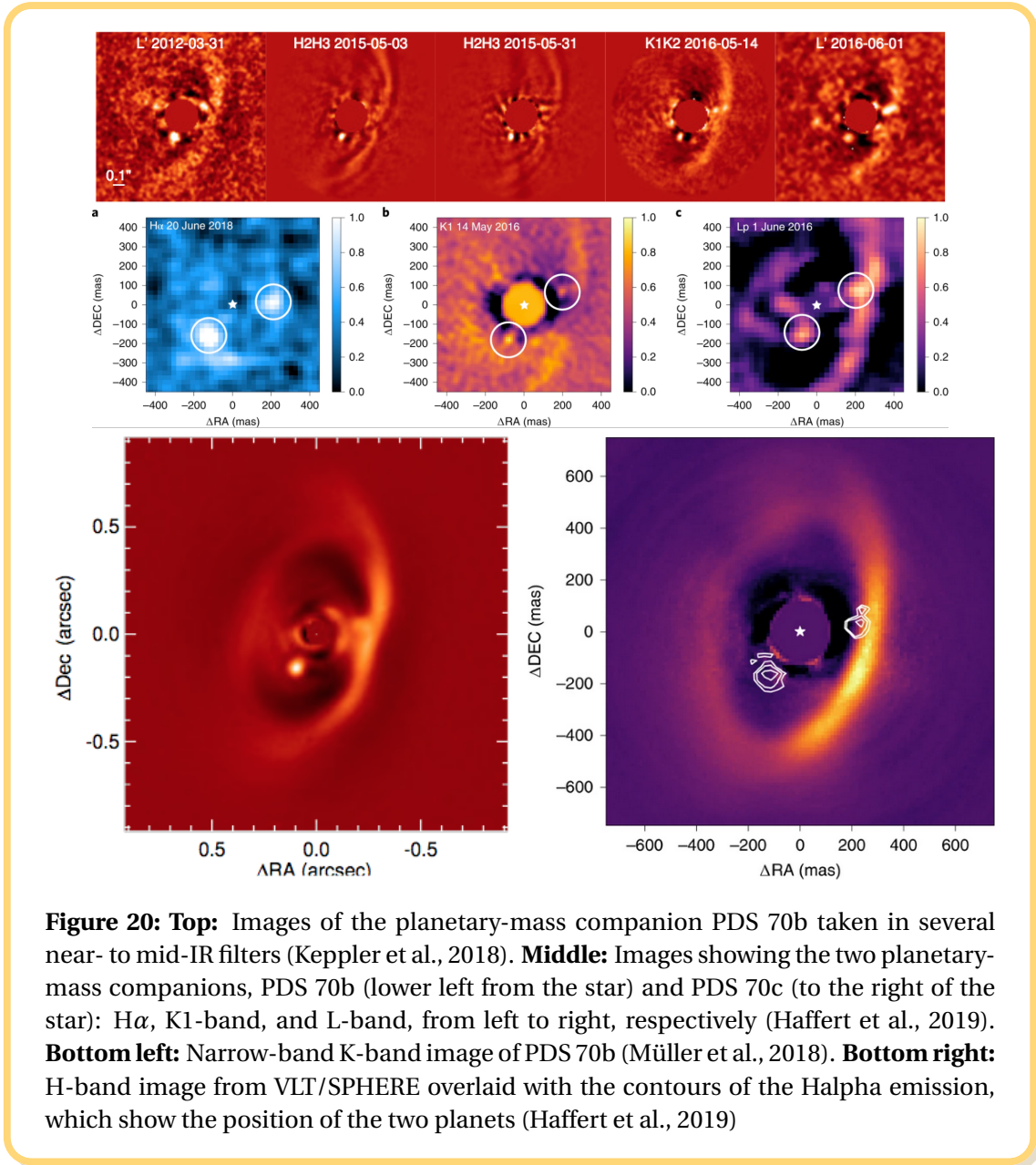

Figure 19: Left: H-band polarized intensity image of PDS 70; **Middle:** SED (data and best-fit model) of PDS 70 (Hashimoto et al., 2012). **Right:** 0.87 mm continuum image of PDS 70 (Long et al., 2018).

Two planetary-mass companions were detected within the cavity of PDS 70, one at about 0.19" (or about 22 AU) from the central star, and one at about 0.25" (or about 28 AU), embedded within a bright region of the dust disk (see Figures 20 and 21). Both young planets were detected in Hα, which implies that they are still accreting. Modeling shows that they are larger and more massive than Jupiter. It is likely that both planets are responsible for clearing out the inner disk gap of PDS 70.
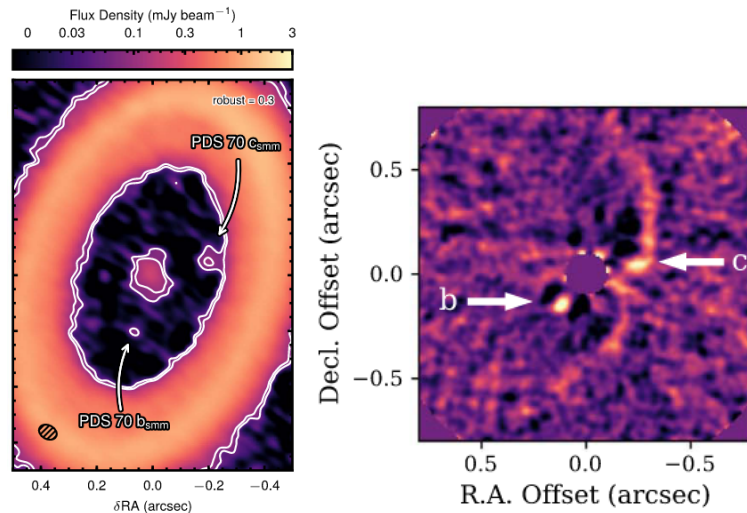

Figure 20: Top: Images of the planetary-mass companion PDS 70b taken in several near- to mid-IR filters (Keppler et al., 2018). **Middle:** Images showing the two planetary-mass companions, PDS 70b (lower left from the star) and PDS 70c (to the right of the star): Hα, K1-band, and L-band, from left to right, respectively (Haffert et al., 2019). **Bottom left:** Narrow-band K-band image of PDS 70b (Müller et al., 2018). **Bottom right:** H-band image from VLT/SPHERE overlaid with the contours of the Halpha emission, which show the position of the two planets (Haffert et al., 2019)

Figure 21: Left: ALMA 0.855 mm image of PDS 70; two compact sources, likely associated with PDS 70b and PDS 70c, are detected within the cavity (Isella et al., 2019). **Right:** Keck/NIRC2 L-band image of PDS 70b and c (Wang et al., 2020).

RADMC-3D MODEL - IMPORTANT FEATURES: The star is taken as a blackbody of temperature 4,400 K. The disk is made out of two sub-disks, both extending from 0.1 AU to 110 AU, and harbouring a wide gap of **radial extent** 1 AU–60 AU and of **depth** 0.001 (the depth being the ratio between in-gap density and out-of-gap density). One disk is made of small 0.1 μm grains and contains 0.1% of the disk's total mass. The other disk is made of bigger 100 μm grains, which contains 99.9% of the disk mass. It is seen at an inclination of 47° from face-on and a position angle of 155°. This system includes a second point source, a **planet** with a nominal mass of 10 Jupiter masses and temperature of 1200 K, separated by 22 AU from the star (so this represents planet PDS 70b).

PYTHON NOTEBOOKS: To study this object, you will work through a Python notebook (either a Jupyter notebook, if you have installed Python, or a Google Colab notebook) and plot various model SEDs and model images (see Figure 22 for an example).
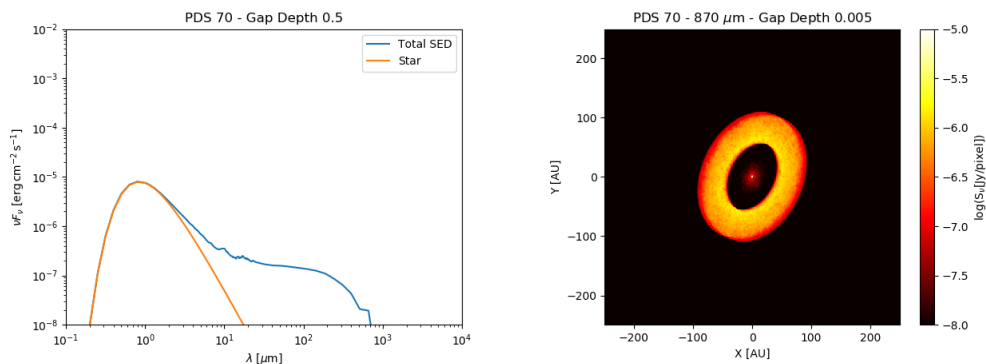

Figure 22: Examples of a model SED plot (**left**) and model image (**right**) for PDS 70. These are the type of plots you will generate in the Python notebook.

As you work through the Python notebook, you will explore the effect of the gap depth and width, as well as the presence of a planet. Please be ready to address the following questions:

QUESTIONS

1. How does the gap width affect the SED?
2. How does the gap depth affect the SED?
3. And how do both of these parameters affect the images?
4. Can you derive the depth and width of the gap from the SED only?
5. Can a planet be detected via the SED?

5 HR 4796

INTRODUCTION   HR 4796A is an A-type star surrounded by a debris disk; it is relatively nearby (72 pc), young (8 Myr), and also has a stellar companion of M spectral type at a distance of 7.7" (Jura et al., 1993). The debris disk consists of second-generation dust, generated in collisions of large remnant bodies (asteroids and comets). The HR 4796A debris disk forms a narrow ring (~ 75 AU semi-major axis), which may be an indication of shepherding by planets; it also has some brightness asymmetries, and the center of the ring seems offset from the star (Wyatt et al., 1999).
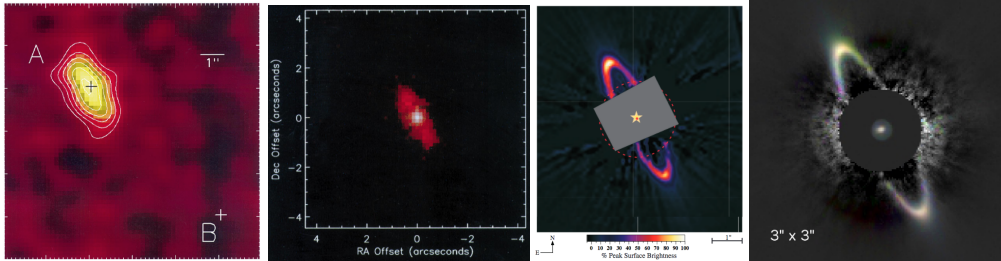
Figure 23: Left: Image of the debris disks around HR 4796A taken at 18 μm (Jayawardhana et al., 1998). **Second from left:** Composite image of HR 4796A taken at 12.5 and 20.8 micron (Koerner et al., 1998). **Second from right:** HST/NICMOS near-IR image of the HR 4796A debris disk (Schneider et al., 2009). **Right:** Gemini/NICI JHK$_s$ false-color image of the HR 4796A debris disk ring (Wahhaj et al., 2014).
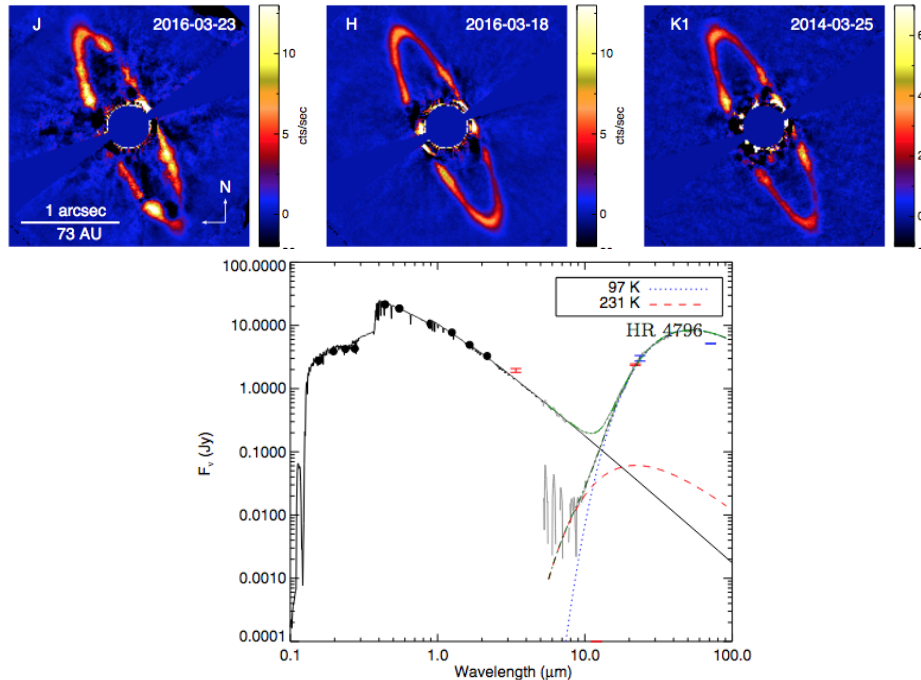

Figure 24: Top: Images of the debris disk of HR 4796A taken in three different near-IR filters with the Gemini Planet Imager (Chen et al., 2020). **Bottom:** SED of HR 4796A; a model that includes the stellar photosphere and two blackbodies (to fit the dust emission) is also shown (Chen et al., 2014)

18

RADMC-3D MODEL - IMPORTANT FEATURES: The star is taken as a blackbody of temperature 10,000 K. The disk extends from 75 AU to 85 AU, i.e., it is **radially centered** at 80 AU, with a total mass of $5 \times 10^{-7} M_\odot$. It has a scale height of 0.01 (reference radius of 100 AU) and a flaring index of 0.1. It is seen at an inclination angle of $77°$ from face-on. The nominal **grain size** is 30 μm.

PYTHON NOTEBOOKS: To study this object, you will work through a Python notebook (either a Jupyter notebook, if you have installed Python, or a Google Colab notebook) and plot various model SEDs and model images (see Figure 25 for an example).
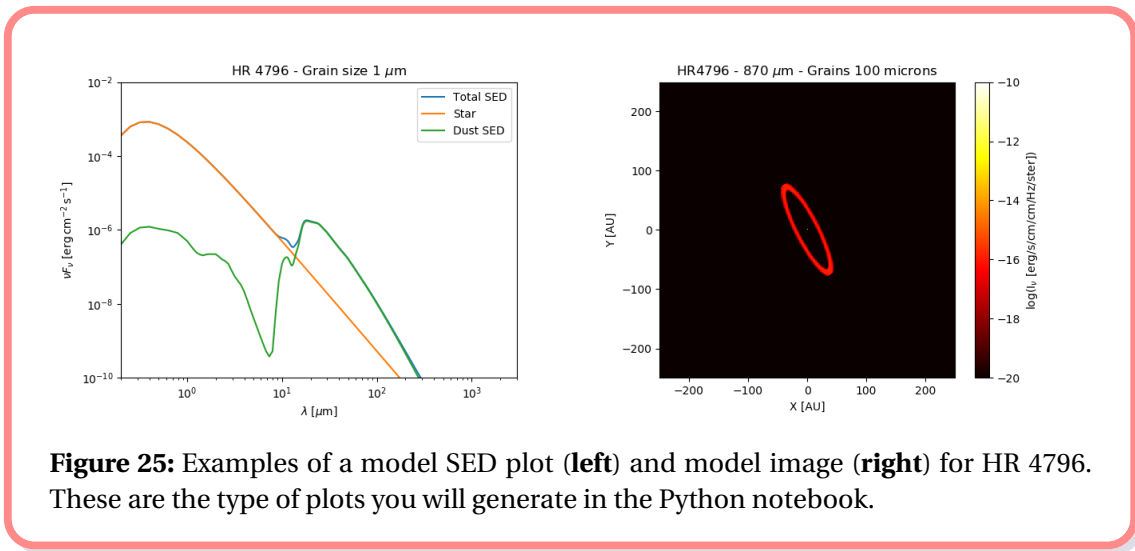

Figure 25: Examples of a model SED plot (**left**) and model image (**right**) for HR 4796. These are the type of plots you will generate in the Python notebook.

As you work through the Python notebook, you will explore the effect of the disk radial location and grain size. Please be ready to address the following questions:

QUESTIONS

1. How does the disk radial distance affect the SED?
2. How does the grain size affect the SED?
3. Can you infer the disk radial distance or grain size from the SED only?
4. How does the grain size affect the images? If you wanted to learn something about grain sizes through images, what would be the best observational strategy?

References

ALMA Partnership, Brogan, C. L., Pérez, L. M., et al. 2015, , 808, L3, doi: 10.1088/2041-8205/808/1/L3

Andrews, S. M., Huang, J., Pérez, L. M., et al. 2018, , 869, L41, doi: 10.3847/2041-8213/aaf741

Anglada, G., López, R., Estalella, R., et al. 2007, , 133, 2799, doi: 10.1086/517493

Arriaga, P., Fitzgerald, M. P., Duchêne, G., et al. 2020, , 160, 79, doi: 10.3847/1538-3881/ab91b1

Aumann, H. H., Gillett, F. C., Beichman, C. A., et al. 1984, , 278, L23, doi: 10.1086/184214

Avenhaus, H., Quanz, S. P., Garufi, A., et al. 2018, , 863, 44, doi: 10.3847/1538-4357/aab846

Backman, D. E., & Paresce, F. 1993, in Protostars and Planets III, ed. E. H. Levy & J. I. Lunine, 1253

Burrows, C. J., Stapelfeldt, K. R., Watson, A. M., et al. 1996, , 473, 437, doi: 10.1086/178156

Carrasco-González, C., Sierra, A., Flock, M., et al. 2019, , 883, 71, doi: 10.3847/1538-4357/ab3d33

Chen, C., Mazoyer, J., Poteet, C. A., et al. 2020, , 898, 55, doi: 10.3847/1538-4357/ab9aba

Chen, C. H., Mittal, T., Kuchner, M., et al. 2014, , 211, 25, doi: 10.1088/0067-0049/211/2/25

Dullemond, C. P., Hollenbach, D., Kamp, I., & D'Alessio, P. 2007, in Protostars and Planets V, ed. B. Reipurth, D. Jewitt, & K. Keil, 555. https://arxiv.org/abs/astro-ph/0602619

Golimowski, D. A., Ardila, D. R., Krist, J. E., et al. 2006, , 131, 3109, doi: 10.1086/503801

Greaves, J. S., Holland, W. S., Moriarty-Schieven, G., et al. 1998, , 506, L133, doi: 10.1086/311652

Haffert, S. Y., Bohn, A. J., de Boer, J., et al. 2019, Nature Astronomy, 3, 749, doi: 10.1038/s41550-019-0780-5

Hashimoto, J., Dong, R., Kudo, T., et al. 2012, , 758, L19, doi: 10.1088/2041-8205/758/1/L19

Hayashi, M., Ohashi, N., & Miyama, S. M. 1993, , 418, L71, doi: 10.1086/187119

Heap, S. R., Lindler, D. J., Lanz, T. M., et al. 2000, , 539, 435, doi: 10.1086/309188

Isella, A., Benisty, M., Teague, R., et al. 2019, , 879, L25, doi: 10.3847/2041-8213/ab2a12

Jayawardhana, R., Fisher, S., Hartmann, L., et al. 1998, , 503, L79, doi: 10.1086/311524

Jura, M., Zuckerman, B., Becklin, E. E., & Smith, R. C. 1993, , 418, L37, doi: 10.1086/187110

Kalas, P., Graham, J. R., & Clampin, M. 2005, , 435, 1067, doi: 10.1038/nature03601

Keppler, M., Benisty, M., Müller, A., et al. 2018, , 617, A44, doi: 10.1051/0004-6361/201832957

Koerner, D. W., Ressler, M. E., Werner, M. W., & Backman, D. E. 1998, , 503, L83, doi: 10.1086/311525

Lagrange, A. M., Langlois, M., Gratton, R., et al. 2016, , 586, L8, doi: 10.1051/0004-6361/201527264

Long, Z. C., Akiyama, E., Sitko, M., et al. 2018, , 858, 112, doi: 10.3847/1538-4357/aaba7c

MacGregor, M. A., Matrà, L., Kalas, P., et al. 2017, , 842, 8, doi: 10.3847/1538-4357/aa71ae

Madlener, D., Wolf, S., Dutrey, A., & Guilloteau, S. 2012, , 543, A81, doi: 10.1051/0004-6361/201117615

McCabe, C., Duchêne, G., Pinte, C., et al. 2011, , 727, 90, doi: 10.1088/0004-637X/727/2/90

Müller, A., Keppler, M., Henning, T., et al. 2018, , 617, L2, doi: 10.1051/0004-6361/201833584

Schneider, G., Weinberger, A. J., Becklin, E. E., Debes, J. H., & Smith, B. A. 2009, , 137, 53, doi: 10.1088/0004-6256/137/1/53

Smith, B. A., & Terrile, R. J. 1984, Science, 226, 1421, doi: 10.1126/science.226.4681.1421

Su, K. Y. L., Rieke, G. H., Malhotra, R., et al. 2013, , 763, 118, doi: 10.1088/0004-637X/763/2/118

Villenave, M., Ménard, F., Dent, W. R. F., et al. 2020, , 642, A164, doi: 10.1051/0004-6361/202038087

Wahhaj, Z., Liu, M. C., Biller, B. A., et al. 2014, , 567, A34, doi: 10.1051/0004-6361/201323335

Wang, J. J., Ginzburg, S., Ren, B., et al. 2020, , 159, 263, doi: 10.3847/1538-3881/ab8aef

Williams, J. P., & Cieza, L. A. 2011, , 49, 67, doi: 10.1146/annurev-astro-081710-102548

Wyatt, M. C., Dermott, S. F., Telesco, C. M., et al. 1999, , 527, 918, doi: 10.1086/308093

Yen, H.-W., Liu, H. B., Gu, P.-G., et al. 2016, , 820, L25, doi: 10.3847/2041-8205/820/2/L25